Earth's Future

RESEARCH ARTICLE
10.1029/2023EF003604

Amplification of Coupled Hot-Dry Extremes Over Eastern Monsoon China

Xinxin Zhang[1], Xihui Gu[1,2,3,4,5,6,7], Louise J. Slater[8], Moctar Dembélé[9], Fatih Tosunoğlu[10], Yansong Guan[1], Jianyu Liu[11], Xiang Zhang[12], Dongdong Kong[1,7], Fenghua Xie[1,7], and Xiongpeng Tang[13,14]

[1]Department of Atmospheric Science, School of Environmental Studies, China University of Geosciences, Wuhan, China, [2]Institute of Arid Meteorology, China Meteorological Administration, Lanzhou, China, [3]The National Key Laboratory of Water Disaster Prevention, Nanjing Hydraulic Research Institute, Nanjing, China, [4]Key Lab of Basin Water Resource and Eco-environmental Science in Hubei Province, Wuhan, China, [5]Key Laboratory of Meteorological Disaster Ministry of Education & Collaborative Innovation Center on Forecast and Evaluation of Meteorological Disasters, Nanjing University of Information Science & Technology, Nanjing, China, [6]SongShan Laboratory, Zhengzhou, China, [7]Centre for Severe Weather and Climate and Hydro-geological Hazards, Wuhan, China, [8]School of Geography and the Environment, University of Oxford, Oxford, UK, [9]International Water Management Institute (IWMI), Accra, Ghana, [10]Department of Civil Engineering, Erzurum Technical University, Erzurum, Turkey, [11]Laboratory of Critical Zone Evolution, School of Geography and Information Engineering, China University of Geosciences, Wuhan, China, [12]National Engineering Research Center of Geographic Information System, School of Geography and Information Engineering, China University of Geosciences, Wuhan, China, [13]Guangdong-Hong Kong Joint Laboratory for Water Security, Beijing Normal University at Zhuhai, Zhuhai, China, [14]Water Security Research Institute, Beijing Normal University at Zhuhai, Zhuhai, China

Abstract High air temperatures and low atmospheric humidity can result in severe disasters such as flash droughts in regions characterized by high humidity (monsoon regions). However, it remains unclear whether responses of hot extremes to warming temperature are amplified on dry days as well as the response of dry extremes on hot days. Here, taking eastern monsoon China (EMC) as a typical monsoon region, we find a faster increase in air temperature on drier summer days, and a faster decrease in atmospheric humidity on hotter days, indicating "hotter days get drier" and "drier days get hotter" (i.e., coupling hotter and drier extremes), especially in southern EMC. The southern EMC is also a hotspot where the coupling hot-dry extremes has become significantly stronger during the past six decades. The stronger hot-dry coupling in southern EMC is associated with anomalies in large-scale circulations, such as reduced total cloud cover, abnormal anticyclones in the upper atmosphere, intense descending motion, and strong moisture divergence over this region. Land-atmosphere feedback enhance the hot-dry coupling in southern EMC by increasing land surface dryness (seen as a decrease in the evaporation fraction). The decreasing evaporation fraction is associated with drying surface soil moisture, controlled by decreases in pre-summer 1-m soil moisture and summer-mean precipitation. Given hot extremes are projected to increase and atmospheric humidity is predicted to decrease in the future, it is very likely that increasing hot-dry days and associated disasters will be witnessed in monsoon regions, which should be mitigated against by adopting adaptive measures.

Plain Language Summary High air temperatures (i.e., hot extremes) and low atmospheric humidity (i.e., dry extremes) are regarded as important metrics affecting human society and the environment in monsoon regions, including food production and natural disasters. Our results show that over eastern monsoon China (EMC), positive responses of hot extremes to warming temperature are magnified on dry days, at the same time, negative responses of dry extremes to warming temperature are enhanced on hot days. In other words, the warming rates of hot extremes per 1°C warming are fastest on dries days, meanwhile, the drying rates of dry extremes per 1°C warming are fastest on hottest days, especially in southern EMC. The southern EMC is also a hotspot where more hot or dry days have become hot-dry days (i.e., stronger coupling of hot and dry extremes) during the past six decades. This stronger coupling of hot and dry extremes can be explained by anomalous large-scale circulations and land-atmosphere feedbacks in southern EMC. Our findings suggest that the positive coupling of hotter and drier extremes should be taken into consideration, and adaptive measures are required to mitigate adverse effects of hot and dry extremes.

Key Points:

- Positive (negative) responses of hot (dry) extremes to warming temperature are amplified on dry (hot) days over eastern monsoon China
- Coupling of hot and dry extremes has strengthened in past six decades in southern EMC
- Coupling of hotter and drier extremes can be explained by anomalies of large-scale circulations and land-atmosphere feedbacks

Supporting Information:

Supporting Information may be found in the online version of this article.

Correspondence to:

X. Gu and F. Xie,
guxh@cug.edu.cn;
xfh5577@126.com

Citation:

Zhang, X., Gu, X., Slater, L. J., Dembélé, M., Tosunoğlu, F., Guan, Y., et al. (2023). Amplification of coupled hot-dry extremes over eastern monsoon China. *Earth's Future*, *11*, e2023EF003604. https://doi.org/10.1029/2023EF003604

Received 16 FEB 2023
Accepted 16 NOV 2023

Author Contributions:

Conceptualization: Xihui Gu, Fenghua Xie
Data curation: Xihui Gu
Formal analysis: Xinxin Zhang, Xihui Gu
Funding acquisition: Xihui Gu
Methodology: Xinxin Zhang, Fenghua Xie
Project Administration: Xihui Gu
Software: Xinxin Zhang
Supervision: Xihui Gu
Visualization: Xinxin Zhang
Writing – original draft: Xinxin Zhang

Writing – review & editing: Xihui Gu, Louise J. Slater, Moctar Dembélé, Fatih Tosunoğlu, Yansong Guan, Jianyu Liu, Xiang Zhang, Dongdong Kong, Fenghua Xie, Xiongpeng Tang

1. Introduction

Significant increases in the magnitude and frequency of hot extremes (i.e., high air temperature) during the late twentieth century have been detected based on both observations and model simulations (Y. Chen, Zhai, & Zhou, 2018; Y. Chen & Zhai, 2017; Y. Sun et al., 2014), and are project to continue in the future (De Luca & Donat, 2023; Li, Zwiers, et al., 2021; J. Wang et al., 2020). Moreover, atmospheric humidity has decreased during 1981–2020 globally (Fang et al., 2022). The frequency of atmospheric aridity enhanced by land-atmosphere feedbacks is projected to increase in the 21st century (Berg et al., 2016; Fang et al., 2022; Feng et al., 2022; J. Liu et al., 2021; S. Zhou, Williams, et al., 2019a). Concurrent hot and dry extremes (i.e., high air temperature accompanied by low atmospheric humidity) can amplify the influence of independently-occurring hot or dry events (Byrne, 2021; Costa et al., 2022; L. Wang, Tong, et al., 2022). For example, exceptional heat and atmospheric dryness amplified drought impacts on losses of primary production in Southwest U.S. in the year 2020 (Dannenberg et al., 2022). In the monsoon region, co-occurrences of hot and dry extremes can accelerate the occurrence of flash droughts and detrimentally affect crop production (Qing et al., 2022). By the end of the 21st century, the co-occurrent hot-dry extremes have an projected widespread increase in frequency and intensity globally (De Luca & Donat, 2023; Mukherjee & Mishra, 2021; Tripathy et al., 2023), and with the higher global warming levels, many regions will experience more extreme hot-dry events (Vogel et al., 2020). The future people and cropland exposure of compound hot-dry events has also been projected to increase, which may bring more risks to our social-ecosystem (Tabari & Willems, 2023). Therefore, it is important to have a deeper understanding of how hot and dry extremes respond to warming temperature.

In regions with climatologically high humidity, such as monsoon regions, numerous studies have focused on the changes and risk of heat stress (i.e., high air temperature with high atmospheric humidity) (X. Liu et al., 2017; Mishra et al., 2020; Ning et al., 2022; X. Wang, Tong, et al., 2022). For example, heat stress might be intensified by increasing heatwaves and irrigation in India, in the South Asia monsoon region (Mishra et al., 2020; Murari et al., 2015). Humid stress also exhibits an intensifying trend in monsoonal southern and eastern China during the past few decades (Xu et al., 2021). However, the increasing attention on heat stress in monsoon regions ignores a fact that observed and simulated atmospheric humidity in these regions has decreased in the past decades (Park et al., 2017; P. Wang, Tong, et al., 2022). Compared with quickly advancing knowledge of heat stress under warming, understanding of hot and dry extremes in monsoon regions still remains limited.

Responses of hot and dry extremes to warming temperature are not independent but coupled, due to the dependence between air temperature and atmospheric humidity (Bourdin et al., 2021; McKinnon & Poppick, 2020; Sun & Oort, 1995). This dependence leads to uneven atmospheric warming and drying across the corresponding temperature and humidity percentiles. For example, Byrne (2021) found that the warming rate of extreme temperature is much higher than that of mean temperature in tropical land due to effects of dry conditions on hot days; Li, Zwiers, et al. (2021) indicated that eastern monsoon China (EMC) has experienced fewer short-duration and more long-duration dry spells under elevated air temperature during 1961–2019. These uneven responses of air temperature and atmospheric humidity to warming temperature raise the question both of how hot extremes may change under dry conditions and dry extremes change on hot days in monsoon regions.

Responses of hot and dry extremes to the warming temperature are mainly shaped by anomalies of large-scale circulations (Espinoza et al., 2019; Horton et al., 2016; Perkins, 2015) and land-atmosphere feedbacks (Miralles et al., 2014; Ukkola et al., 2018; S. Zhou, Williams, et al., 2019a). For instance, hot extremes in the mid-high latitudes are associated with the blocking high, which leads to high air temperature by modifying the position of the jet stream and preventing propagation of weather systems (Pfahl et al., 2015; Pfahl & Wernli, 2012). Heatwaves in Southern China are linked with an eastward extension of the South Asian high in the upper level of the atmosphere, a westward extension of the western North Pacific subtropical high in the middle level, and a low-level anticyclonic anomaly (Luo, Wu, et al., 2022). Land-atmosphere feedbacks play another important role in enhancing the occurrence of hot and dry extremes (Berg et al., 2016; McKinnon et al., 2021; S. Zhou, Williams, et al., 2019a). Summer mean precipitation deficits could increase the frequency of hot-dry events (Bevacqua et al., 2022), by causing soil moisture depletion (Zhou et al., 2019). As the soil dries out, decreased actual evaporation cannot meet the atmospheric demand on hot days, resulting in drying and intensified heating of the atmosphere (Miralles et al., 2019) and then increasing likelihood of concurrent hot and dry extremes.

EMC, which is home to 95% of China's population and contributes more than 95% of gross domestic product (X. Gu et al., 2020), is a typical monsoon region. This monsoon region has witnessed more frequent and intense hot

extremes (Y. Sun et al., 2014) and decreased atmospheric humidity (Park et al., 2017). However, the coupling hot and dry extremes in EMC is still not well understood. In this study, we set EMC as the study region and aim to address the following questions.

- Is there an amplified warming (drying) on dry (hot) days (i.e., hot-dry coupling) over EMC?
- If yes, is the hot-dry coupling stronger (i.e., hotter days get drier and drier days get hotter) in recent decades over EMC?
- If yes, what are the possible mechanisms responsible for the coupling of hot and dry extremes?

2. Study Region and Data

2.1. Study Region

The monsoon region in China (i.e., EMC) is defined as the area where the precipitation difference between summer and winter seasons (i.e., June-August and December-February, respectively) exceeds 2.0 mm/day and the summer precipitation contributes more than 55% of annual precipitation total (B. Wang et al., 2012; Wu et al., 2019; Zhang et al., 2018). In this study, the boundaries of EMC are obtained from Wu et al. (2019) (Figure S1 in Supporting Information S1, Wu et al., 2019). The boundaries of EMC have been used in many studies (Li, Zwiers, et al., 2021; L. Wei et al., 2021).

2.2. Station-Based Weather Observations

We obtained long-term daily observations at 2,481 weather stations across China from the China Meteorological Administration. Among the 2,481 stations, there are 2,060 stations across the EMC region. The following variables are used in our study: near-surface air temperature (SAT; units: °C), near-surface relative humidity (RH; units: %), near-surface air pressure (PRS; units: hPa), and precipitation (PRE; units: mm). Quality control and homogenization of recently released datasets have been performed according to the Guidelines on the Quality Control of Surface Climatological Data (L. Cao et al., 2016; Ren et al., 2015).

Daily SAT, RH, and PRS are used to calculate specific humidity (Q; units: g/kg) and vapor pressure deficit (VPD; units: hPa). Stations must contain observations of all three variables during summer seasons of 1961–2020, and are selected according to the following criteria: a summer season with no more than three missing days for any of the three variables; and, stations with no more than five missing summer seasons. After all filtering steps, a total of 1,408 stations remain across EMC. Stations with less than 1% of missing data account for 67%–91% of the total 1,408 stations (depending on the variable; see Figure S1 in Supporting Information S1), confirming that the new version of the observed dataset is of the greatest completeness and quality, relative to those released before (Huang et al., 2022).

2.3. ERA5 Reanalysis Data

Hourly 2-m SAT (units: °C), 2-m dewpoint temperature (Td; units: °C), RH (units: %), and PRS (units: hPa), obtained from the ERA5 reanalysis data (Hersbach et al., 2020), are used to calculate Q and VPD. Hourly air temperature (units: °C), RH, PRS and vertical velocity (units: Pa/s) at multiple layers (i.e., 1,000–100 hPa), hourly total cloud cover (units: %), 200-hPa geopotential height (units: m) and wind field (units: m/s), 500-hPa vertical velocity (units: Pa/s), the vertical integral of moisture divergence (VIMD; units: kg/m^2) and the vertical integral of eastward (northward) water vapor flux (units: kg/m/s) are used to investigate large-scale circulations. Hourly values of these variables are averaged into daily mean values. Besides these hourly values, we also collect monthly values of total precipitation (units: mm), volumetric soil moisture at 0–7 cm and 0–1 m (units: m^3/m^3), surface latent heat flux (Units: W/m^2), and surface sensible heat flux (Units: W/m^2) to analyze land-atmosphere feedbacks. To be consistent with the units of precipitation, the units of soil moisture are converted to mm. The ERA5 reanalysis data of all these variables are obtained at a spatial resolution of 0.25° × 0.25° during the summer seasons of 1961–2020. ERA5 reanalysis utilizes advanced data assimilation techniques to effectively integrate data from multiple observational sources, thereby enhancing data consistency and accuracy (Hersbach et al., 2020). ERA5 reanalysis dataset also provides a set of data with prolong temporal coverage (Bell et al., 2021) and high spatial resolution.

Table 1
The Definition of Hot Days, Dry Days and Hot-Dry Days

Classification	Definition
hot day	SAT>90th SATref
Q-based dry day	Q < 10th Qref
VPD-based dry day	VPD>90th VPDref
Q-based hot-dry day	SAT>90th SATref and Q < 10th Qref
VPD-based hot-dry days	SAT>90th SATref and VPD>90th VPDref

3. Methods

3.1. Calculating Specific Humidity and Vapor Pressure Deficit

Diverse humidity variables (such as Q, RH, and VPD) can be used to describe atmospheric humidity. Vapor pressure deficit (VPD) measures the difference between actual atmospheric humidity level and saturation humidity, while specific humidity (Q) describes the actual water content of the wet air. Thus, we examine two different humidity indicators, including specific humidity (Q; units: g/kg) and vapor pressure deficit (VPD; units: hPa), to explore the relationship between atmospheric humidity and air temperature in EMC. The two humidity indicators are computed as follows (Bolton, 1980; Luo & Lau, 2019; McElhinny et al., 2020):

$$\begin{cases} \mathrm{Es} = 6.11 \times \exp\left(\frac{17.67\times \mathrm{SAT}}{243.5+\mathrm{SAT}}\right) \\ \mathrm{Ea}_{\mathrm{obs}} = \mathrm{Es} \times \frac{\mathrm{RH}}{100} \\ \mathrm{Ea}_{\mathrm{ERA5}} = 6.11 \times \exp\left(\frac{17.67\times \mathrm{Td}}{243.5+\mathrm{Td}}\right) \\ \mathrm{VPD} = \mathrm{Es} - \mathrm{Ea} \\ \mathrm{Q} = \frac{622\times \mathrm{Ea}}{\mathrm{PRS}-0.378\times \mathrm{Ea}} \end{cases} \quad (1)$$

where Es is saturated vapor pressure (units: hPa); and Ea is actual vapor pressure (units: hPa). RH is used to estimate Ea in observed data, and Td is used to calculate Ea in ERA5 reanalysis data.

The climatological SAT in EMC exhibits a zonal distribution in which lower latitudes have higher air temperature and higher latitudes have lower air temperature (Figure S2a in Supporting Information S1). The climatological Q in this region has a similar distribution to SAT, that is, high Q in the southern regions and low Q in the northern regions (Figure S2b in Supporting Information S1). The distribution of climatological VPD is uneven, that is, high VPD in central EMC and low VPD in northern and southwestern EMC (Figure S2c in Supporting Information S1). The distributions of climatological SAT/Q/VPD based on ERA5 data are consistent with those based on observations (Figure S2d-S2f in Supporting Information S1).

3.2. Definitions of Hot Days, Dry Days, and Hot-Dry Days

In this study, we set the period 1981–2010 as the reference period. Each percentile (i.e., 10th, 20th, 30th, …, 90th) of SAT/Q/VPD on a calendar day is determined by ranking the 15-day values (i.e., 7 days before and after the given calendar day) during the reference period (a total of 15×30 = 450 values). A hot day during the period of 1961–2020 is defined as a day with SAT exceeding its 90th percentile value (i.e., 90th SATref) over the reference period (see Table 1). Likewise, a Q/VPD-based dry day is a day with Q/VPD below/exceeding the corresponding tenth/90th percentile value (i.e., 10th Qref/90th VPDref). A hot-dry day is defined as a co-occurring hot and dry day (e.g., De Luca & Donat, 2023). Therefore, daily Q and VPD are divided into two groups representing the background conditions (with hot days removed) and hot-day conditions, respectively. Daily SAT is also divided into two groups representing the background conditions (with dry days removed) and dry-day conditions, respectively.

3.3. Definition of Amplification Index

The amplification index, first defined by McKinnon et al. (2021), is employed in our study to evaluate whether hot days are becoming drier or dry days are becoming hotter. Specifically, the Q/VPD-based amplification index (i.e., Q1/VPD1) is defined as the ratio of the number of annual Q/VPD-based hot-dry days to annual total hot days, and ranges from 0 to 1, with larger values indicating that more hot days are becoming drier. Similarly, Q2/VPD2 is defined as the ratio of the number of annual Q/VPD-based hot-dry days to annual Q/VPD-based dry days, with larger values indicating that more dry days are becoming hotter.

10.1029/2023EF003604

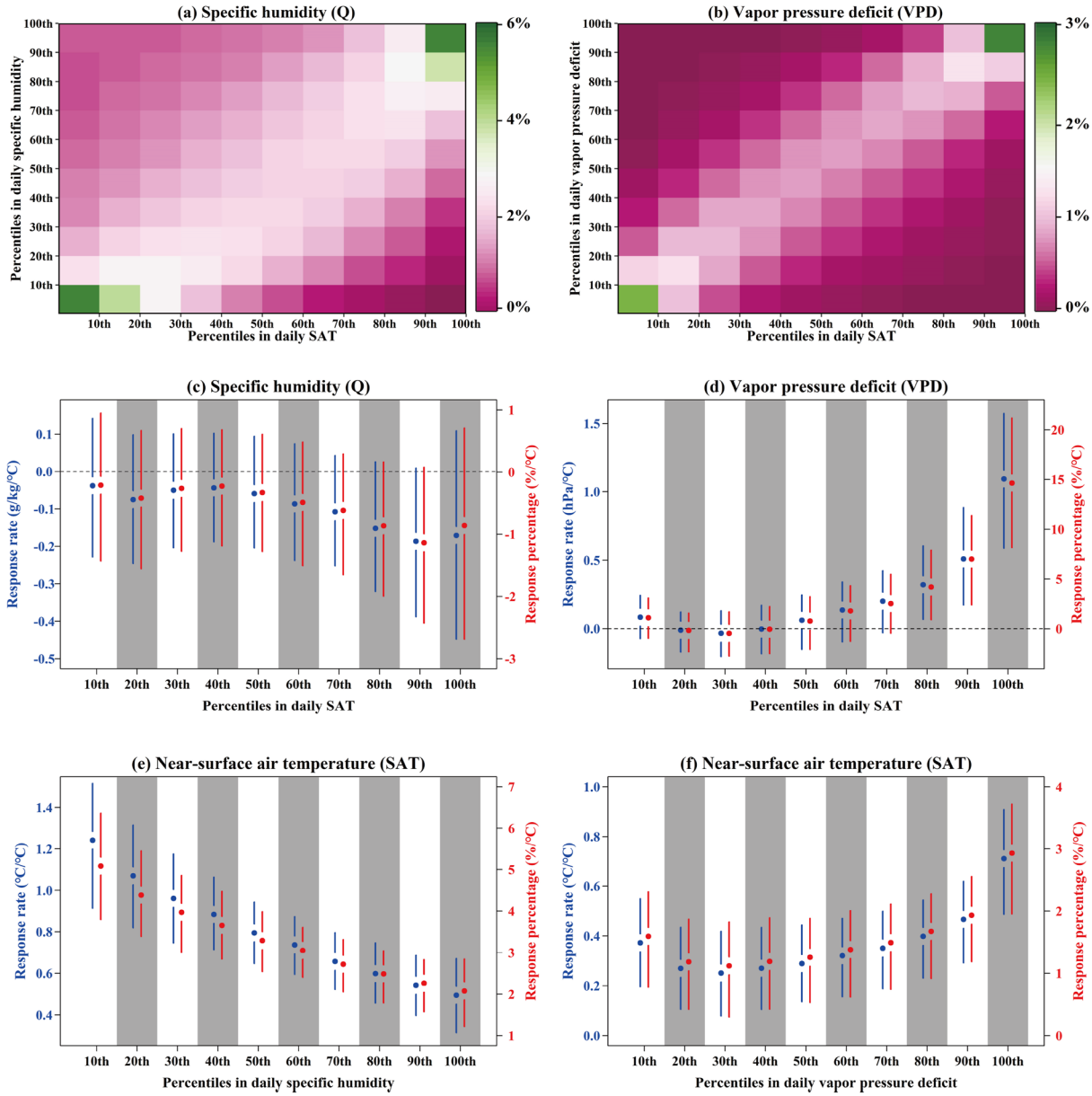

Figure 1. Coupling of near-surface air temperature (SAT) and near-surface specific humidity (Q)/vapor pressure deficit (VPD) at 1,408 stations across eastern monsoon China (EMC) during the summer seasons of 1961–2020. In panel a/b, daily SAT and Q/VPD are each binned into 10 percentiles, and the mean probability of each percentile bin is counted. In panel c/d, matchsticks show response rates (percentages) of Q/VPD to summer-mean SAT on the days within different SAT percentiles. Taking panel c as an example, Q values on the days with SAT between two SAT percentiles (i.e., 0–10th, 10–20th, …, 90–100th) are averaged in each summer season, and the obtained annual Q time series is linearly fitted against summer-mean SAT to compute the response rate (i.e., regression coefficient) and response percentage (i.e., regression coefficient normalized by climatological mean). In panel e/f, matchsticks show response rates (percentages) of SAT to summer-mean SAT on the days within different Q/VPD percentiles. In panel c–f, middle points are the estimates and sticks are the corresponding 25%–75% range. In panels a–f, the approach to calculate SAT/Q/VPD percentiles is described in Section 3.2.

3.4. Statistical Analysis

In order to explore the relationship between different percentile of SAT and Q/VPD in EMC, we binned daily SAT and Q/VPD observations at the 1,408 stations across EMC during 1961–2020 into 10 × 10 percentiles and assessed the co-occurrence probability of SAT and Q/VPD within each of the percentile bins (Figures 1a and 1b).

We use the linear regression method to calculate response rate and response percentage. We group daily Q and VPD in each summer season during 1961–2020 into 0–10th, 10–20th, …, 90–100th percentile intervals of SAT,

and regressed them on summer-mean SAT to obtain the response rate, respectively (Figures 1c and 1d). Taking Figure 1c as an example, Q values on the days with SAT between two SAT percentiles (i.e., 0–10th, 10–20th, …, 90–100th) are averaged in each summer season, and the obtained annual Q time series is linearly fitted against summer-mean SAT to compute the response rate (i.e., regression coefficient) and response percentage (i.e., regression coefficient normalized by climatological mean).

4. Results

4.1. Amplified Atmospheric Warming/Drying on Dry/Hot Days

First, the relationship between SAT and Q/VPD is examined using station-based observations as well as the ERA5 reanalysis data. A positive dependence between SAT and Q/VPD is evident, that is, there is a greater probability of co-occurrence and bimodality toward both ends of the distribution: high SAT-high Q/VPD and low SAT-low Q/VPD. This dependence between SAT and Q/VPD is validated by the ERA5 reanalysis data (Figures S3a–S3b in Supporting Information S1). The SAT-Q relationship meets the theory that specific humidity will generally increase with warming temperature due to the Clausius-Clapeyron relationship (Held, 2006; Sippel et al., 2020). This dependence between SAT and Q/VPD implies that responses of SAT (Q/VPD) to warming temperature may be nonlinear and nonmonotonic across different air temperature (atmospheric humidity) conditions.

To quantitatively estimate response rates of Q/VPD to warming temperature across SAT percentiles, a linear regression model is established between Q/VPD within each SAT percentile and summer-mean SAT. The regression coefficient indicates the response rate of Q/VPD to SAT. Q (VPD) response rates to warming temperature vary distinctly across the SAT percentiles, and show an asymmetrical distribution with air temperature, that is, the response rates of Q (VPD) have higher negative (positive) values, when the SAT percentile is larger (Figures 1c and 1d). These results imply that hotter air temperature may amplify the negative (positive) response of Q (VPD) to warming temperature. This phenomenon can be simply termed as "hotter days get drier".

In the same way, SAT responses to warming temperature are also asymmetrically distributed across the Q/VPD percentiles (Figures 1e and 1f). Positive responses of SAT are more intense in lower Q percentiles and higher VPD percentiles, implying that air temperature rises faster in a drier atmosphere (i.e., with lower Q or higher VPD). This phenomenon can be simply described as "drier days get hotter". We also normalize the response rate as a response percentage, which removes the impact of magnitudes of SAT/Q/VPD across the corresponding percentiles. The results of Q/VPD response percentages are in accordance with the response rates, as well as the results of SAT response (Figures 1c–1f). Both the "hotter days get drier" and "drier days get hotter" phenomena found in station-based observations are consistent with those found in the ERA5 reanalysis data (Figure 1c–1f and Figures S3c–S3f in Supporting Information S1).

We then compare the spatial responses of observed Q/VPD to warming temperature between background and hot-day conditions, and SAT response to warming temperature between background and dry-day conditions (Figure 2). The Q response to warming temperature clearly exhibits opposite behaviors between background conditions and hot days across EMC (Figures 2a and 2b). The response of Q to warming temperature is positive at most of stations (i.e., at 81% of the 1,408 stations in Figure 2a) under background (hot days removed, see Section 3.2) conditions. Conversely, on hot days, the response of Q to warming temperature becomes negative at most stations (i.e., at 66% of the 1,408 stations in Figure 2b). The areas with the most pronounced shifts (i.e., from positive to negative) in Q responses are located in southern EMC where Q experiences a decrease per 1°C warming on hot days at most stations (i.e., at 77% of the 716 stations across southern EMC in Figure 2b).

For VPD, widespread positive responses are found under background conditions across the whole EMC (Figures 2c and 2d), and these positive responses are visibly stronger on hot-day conditions (at 93% of the 1,408 stations), especially in southern EMC (at 95.5% of the 716 stations in this region). The responses of Q/VPD to warming temperature under background conditions across EMC are significantly negative/positive with climatological mean SAT (see the scatterplots in Figures 2a and 2c), and this negative/positive dependence is even stronger under hot-day conditions (see the scatterplots in Figures 2a–2d), suggesting that areas with higher climatological mean SAT (such as southern EMC; see Figures S2a–S2b in Supporting Information S1) are the areas with faster negative/positive Q/VPD responses. These results indicate that atmospheric drying for both Q and VPD is amplified on hot days, especially in southern EMC, which is further corroborated by Q/VPD responses based on the ERA5 reanalysis data (Figures S4a–S4d in Supporting Information S1).

10.1029/2023EF003604

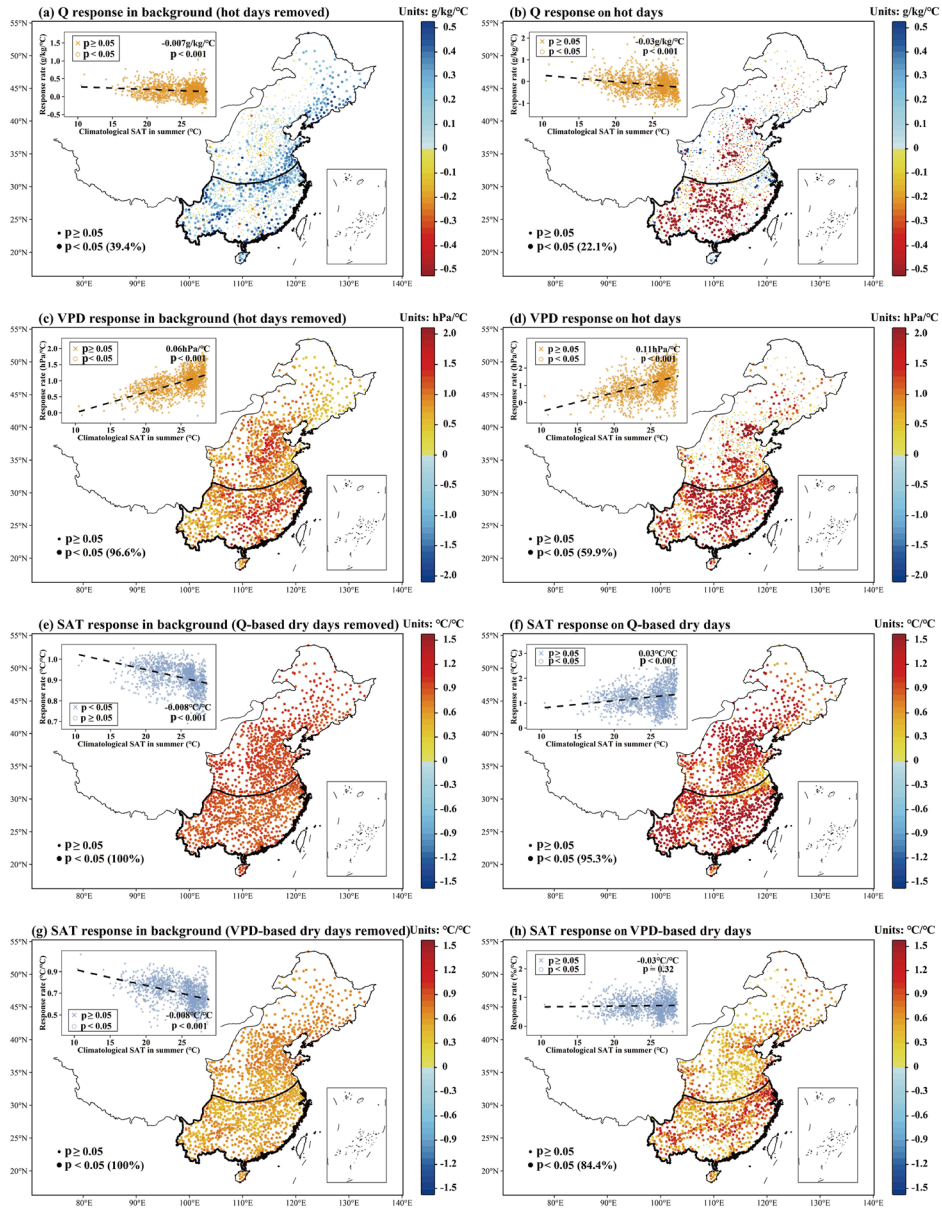

Figure 2. Response rates of Q/VPD (SAT) under background and hot-day (dry-day) conditions to summer-mean SAT across EMC during summer seasons of 1961–2020. Panels a and b are spatial distributions of response rates of Q under background (hot days removed) and hot-day conditions, respectively. Panels c and d are the same as panels a and b, but for VPD. Panels e and f are spatial distributions of response rates of SAT under background (Q-based dry days removed) and Q-based dry-day conditions, respectively. Panels g and h are the same as panels e and f, but for VPD-based dry days. The definitions of hot/dry days can be seen in Section 3.2. For scatterplots in panels a–h, dashed lines are the estimated linear regression relations of the response rates and climatological summer SAT for all stations. The area enclosed by the bold black line indicates the southern EMC region.

We also detect the response in SAT to warming temperature on dry days compared to corresponding background conditions (Q-based or VPD-based dry days removed) during 1961–2020 in EMC (Figures 2e–2h). The responses of SAT to warming temperature increase faster on both VPD-based and Q-based dry days than under background conditions, especially in southern EMC. The response differences of SAT between dry days and background conditions show that changes in SAT are more sensitive to warming when the air is dry, confirming that SAT increases are amplified under low humidity conditions. Moreover, there is a negative relationship between SAT responses under background conditions and climatological mean SAT (see the scatterplots in Figures 2e and 2g), indicating that regions with climatologically-lower SAT have a larger SAT response to warming, which

is consistent with the finding that the strongest warming rate in recent decades has occurred in mid-high latitudes (Y. Xie et al., 2016). However, this negative relationship is largely weakened on VPD-based dry days, and turns to become significantly positive on Q-based dry days (see the scatterplots in Figures 2f and 2h), suggesting that the SAT on dry days rises faster over lower latitudes with higher climatological SAT, such as southern EMC. The observations-based results shown in Figure 2 are consistent with the ERA5-based results shown in Figure S4 in Supporting Information S1.

Overall, hot and dry extremes are positively coupled under elevating air temperature in EMC. This coupling of hot and dry extremes is also reflected by the asymmetrical shift toward faster responses of atmospheric warming/drying on drier/hotter days. Compared with background conditions, atmospheric warming/drying is amplified on hot/dry days, especially in southern EMC, which we describe as the "hotter days get drier" and "drier days get hotter" phenomena.

4.2. Stronger Coupling of Hot and Dry Extremes

As both station-based observations and the ERA5 reanalysis data reveal a dependence between SAT and Q/VPD (especially the strong coupling between hot and dry extremes), we develop amplification indices (see Section 3.3) to evaluate long-term changes in this coupling over EMC during the summer seasons of 1961–2020 (Figure 3). Over the whole EMC, stations with positive trends in Q1 and VPD1 account for 63% and 68% of the total stations during 1961–2020, respectively (Figures 3a and 3c). The significant positive trends occur mainly at stations in southern EMC; specifically, 201/288 (i.e., 25.8%/41.5% of) stations show significant increasing Q1/VPD1 in southern EMC. The significant increasing trends in both Q1 and VPD1 over southern EMC indicate that more hot days have become drier in this region during 1961–2020. At the same time, positive tendencies are also found in Q2/VPD2 across EMC, especially in southern EMC where 41.5%/35.8% of the stations show significant increasing Q2/VPD2 (Figures 3b and 3d). The significant increasing trends in Q2/VPD2 over southern EMC indicate that more dry days have become hotter in this region during 1961–2020. Therefore, southern EMC is a hotspot where the hot-dry coupling has become stronger during the past six decades.

We now exclusively focus on the southern EMC region, and estimate trends in the regional mean of Q1, Q2, VPD1, and VPD2 during 1961–2020 based on the observed data and ERA5 reanalysis data, respectively (see line charts in Figures 3a–3d). Trends in regional mean time series confirm that these four amplification indices have significantly increased in southern EMC during 1961–2020, notably in the last 20 years. The regional mean time series over southern EMC from the ERA5 reanalysis data are significantly correlated to the mean computed from station-based observations for all four amplification indices (the range of Spearman's r values is 0.46–0.87 and all p values less than 0.001), suggesting that the ERA5 reanalysis data appropriately captures changes in the four amplification indices in southern EMC.

This noteworthy increase in earlier 2000s have a similar trend with characteristic of heatwaves in EMC (Xie et al., 2020; Zhou et al., 2016), especially in southern EMC (You et al., 2017). After 2000, the frequency, duration and maximum intensity of heatwaves in EMC have significantly increased (Ji et al., 2023; Liang et al., 2022; Yao et al., 2023). Therefore, more frequent and severe heatwaves since 2000 may cause an increase incidence of hot-dry days, leading to a rapidly rising trend of amplification indices. Meanwhile, soil moisture at both surface and root zone layers in the southern EMC region has been detected to be decreasing during the past decades, especially after 2000 (Cai et al., 2017; X. Chen et al., 2016). Due to the soil moisture-VPD coupling effects, that is, lower soil moisture associated with higher VPD (L. Liu et al., 2020; Seneviratne et al., 2010; S. Zhou, Zhang, et al., 2019), the EMC region may suffer more days with a drier atmosphere in recent 20 years, which may contribute to the increase in amplification indices.

The southern EMC is a region affected by frequent heavy precipitation (HP) events (L. Wei et al., 2021; Wu et al., 2019). On the one hand, increases in sequential HP-heatwave events have been detected in southern EMC in recent decades and are projected to continue in the warming future (Y. Chen et al., 2021; Liao et al., 2021). On the other hand, Dai et al. (2020) indicated that these HP events may cause atmospheric drying in the following days by removing moisture from the atmosphere. Thus, we identify hot-dry days preceded by HP events (referred to as "HP-preceded hot-dry days") to investigate the impacts of HP events on increasing hot-dry days in southern EMC. We first identify all precipitation events, and select HP events whose peak values exceed the 80th percentile of all summer-season values during the reference period of 1981–2010. The 80th percentile is chosen as

10.1029/2023EF003604

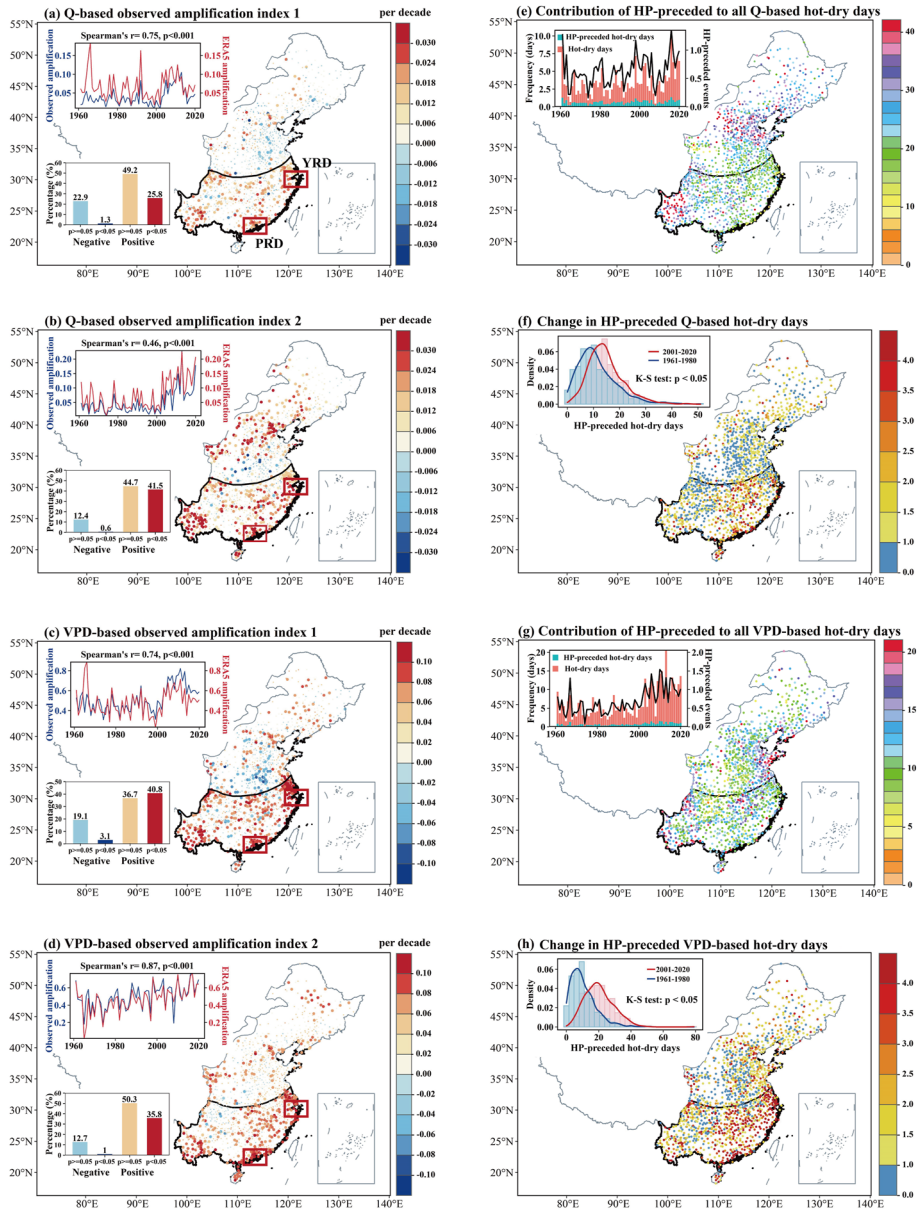

Figure 3. Changes in hot-dry coupling defined by amplification indices (left column) and in the number of hot-dry days preceded by heavy precipitation ("HP-preceded hot-dry day"; right column) over EMC during summer seasons of 1961–2020. In panels a–d, trends in four amplification indices (i.e., Q1, VPD1, Q2, and VPD2) are estimated using the Mann-Kendall method (Hamed & Ramachandra, 1998); large points indicate trends at the 0.05 significance level. In the upper-left sub-panel of panels a–d, blue (red) lines are regional mean values of Q1, Q2, VPD1, and VPD2 over southern EMC based on station-based observations (the ERA5 reanalysis data). In panels a–d, r is Spearman's rank correlation coefficient computed between the blue and red lines and p is the corresponding significance. In the bottom-left sub-panel of panels a–d, barplots show percentages of stations with a significant positive trend (red), insignificant positive trend (orange), significant negative trend (dark blue) and insignificant negative trend (sky blue) in amplification indices over southern EMC. The areas enclosed by red boxes are the Yangtze River Delta (YRD; the northern box) and the Pearl River Delta (PRD; the southern box), respectively. If a HP event occurs in the 5 days prior to a hot-dry event, we define this as a HP-preceded hot-dry event. Contributions of HP-preceded hot-dry days to all hot-dry days are shown in panels e and g (see colorbar). Ratios of HP-preceded hot-dry days and total hot-dry days are shown for two 20-year periods (i.e., 1961–1980 and 2001–2020) in panels e and g (see colorbars). Barplots in panels e and g show the regional mean HP-preceded (green) and total hot-dry days (red) in southern EMC; and the black solid lines are regional mean HP-preceded hot-dry events. Probability density functions (PDFs) in panels f and h show the number of HP-preceded hot-dry days at each station during the two 20-year periods, and the difference of PDFs between the two periods is tested using the Kolmogorov-Smirnov method (Massey, 1951; Mazdiyasni & AghaKouchak, 2015).

the threshold because southern EMC is a region of abundant precipitation in the summer season, where a large number of HP events can be identified (a higher percentile does not alter our results but decreases the number of identified HP-preceded hot-dry days). If a hot-dry event occurs within 5 days of a HP event, we define it as a HP-preceded hot-dry event. The threshold of 5 days is chosen in line with previous studies, where other time lags (such as three or 7 days) were tested and revealed little impact on the identification of sequential events (Y. Chen et al., 2021; L. Gu et al., 2022; Li et al., 2022; Liao et al., 2021).

Using the regional mean, we find significantly increasing trends in the frequency of both hot-dry days and HP-preceded hot-dry events in southern EMC (see top-left subpanel of Figures 3e and 3g). The concurrent increases in hot-dry days and HP-preceded hot-dry events imply increasing HP events in southern EMC (X. Gu et al., 2017) may be responsible for the increase in hot-dry days in this region. This finding is also confirmed by the ratios of HP-preceded hot-dry days between two 20-year periods (i.e., 1961–1980 vs. 2001–2020); the ratios show that HP-preceded hot-dry days at 31% (53%) of stations in the recent period is twofold more than that of the early period (Figures 3f and 3h). The probability density function (PDF) of HP-preceded hot-dry days during 2001–2020 is significantly shifted to the right, relative to the PDF for 1961–1980, furthermore suggesting that southern EMC has experienced a greater number of HP-preceded hot-dry days in the last 20 years (see PDFs in Figures 3f and 3h). Nevertheless, the impacts of HP events on increasing hot-dry days in southern EMC are limited, because the contribution of HP-preceded hot-dry days to all Q-based (VPD-based) hot-dry days shows that on average only 25% (12%) of hot-dry days are linked to HP events in southern EMC (Figures 3e and 3g).

4.3. Physical Mechanisms for the Coupling of Hotter and Drier Extremes

Besides the small contribution of HP-preceded hot-dry days to all hot-dry days, anomalies of large-scale circulations (such as cloud cover, geopotential height, vertical velocity, and vertical integral of moisture divergence; Luo & Lau, 2017, 2018; Singh et al., 2014) and land-atmosphere feedbacks (such as evaporation and soil moisture; Costa et al., 2022; McKinnon et al., 2021; Ukkola et al., 2018) may play a key role in the occurrence of hot and dry extremes and their responses to warming temperature. We therefore turn to exploring whether anomalies of large-scale circulations and land-atmosphere feedbacks are responsible for the increases in hot-dry days in southern EMC.

We first explore the role of large-scale circulations in the coupling of hot and dry extremes in southern EMC (Figure 4 and Figure S5 in Supporting Information S1). To understand the behavior of air temperature and atmospheric humidity on hot-dry days, we calculate composite anomalies of SAT, Q, RH, and VPD on VPD-based/Q-based hot-dry days over southern EMC, and depict the vertical structure (i.e., 1,000 hPa–100 hPa) of their anomalies (Figures 4a, 4d and S5a-S5d in Supporting Information S1). During hot-dry days, significant positive air temperature anomalies can be seen over southern China and form a warm core in the northern part of southern EMC (Figure 4a and Figure S5a in Supporting Information S1). At the same time, reduced Q is observed in the lower atmosphere over southern EMC; and the negative Q anomalies are strongest in the middle atmosphere (at 500–600 hPa; Figure 4b and Figure S5b in Supporting Information S1). The reduced Q is companied by significant negative RH anomalies (Figure 4c and Figure S5c in Supporting Information S1) and positive VPD anomalies (Figure 4d and Figure S5d in Supporting Information S1). From the vertical anomalies, the strongest RH (VPD) decreases (increases) happen in the mid-upper (lower) level (sub-panels in Figures 4c and 4d and Figure S5c-Sd in Supporting Information S1). Both the horizonal and vertical distribution of anomalies in air temperature and atmospheric humidity indicate that hot-dry extremes can be regional events with impacts over areas as large as the entire southern EMC.

We then examine the anomaly patterns of large-scale circulations on hot-dry days (Figures 4e–4h and Figures S5e–S5h in Supporting Information S1). The hot-dry days in southern EMC are accompanied with reduced total cloud cover in this region. The reduction in cloud cover can increase solar shortwave radiation reaching the surface, which warms the near-surface air temperature and may increase the occurrence of hot days (Figure 4e and Figure S5e in Supporting Information S1; R. Chen, Zhai, & Zhou, 2018; Luo, Wu, et al., 2022; Luo & Lau, 2017). The composite geopotential height and wind field anomalies in the upper (200 hPa) atmosphere depict a high-pressure center and anticyclone over China (Figure 4f and Figure S5f in Supporting Information S1), in accordance with the presence of positive air temperature anomalies in the upper level of the atmosphere (sub-panel in Figure 4a and Figure S5a in Supporting Information S1). The strong anticyclone blocks the ascending motion in southern EMC, such that an unusual descending motion occurs across the whole atmosphere

10.1029/2023EF003604

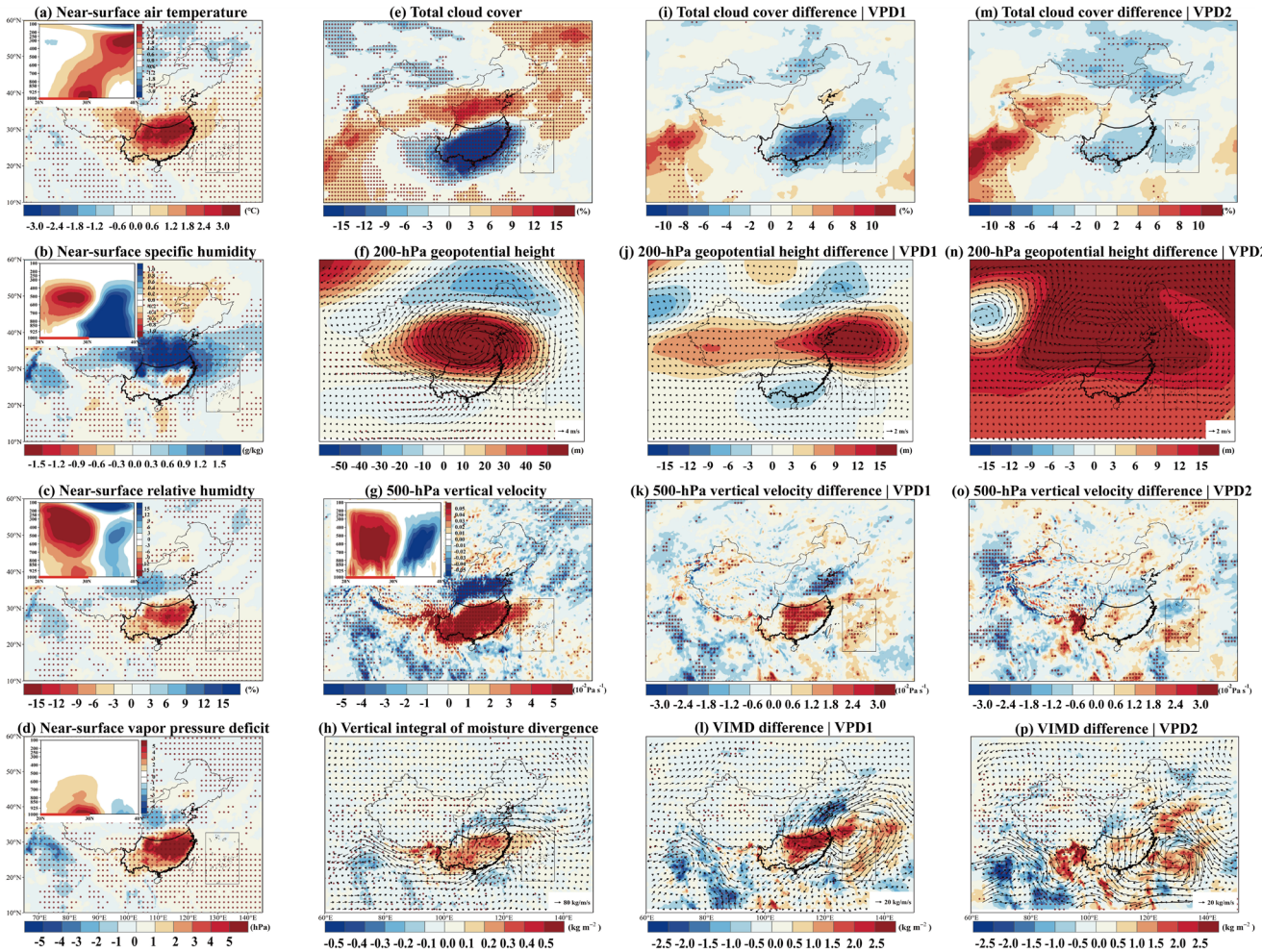

Figure 4. Anomaly patterns of large-scale environmental conditions on VPD-based hot-dry days over southern EMC during summer seasons of 1961–2020 based on the ERA5 reanalysis data. Panels a–d are composite anomalies of daily SAT, Q, relative humidity, and VPD on hot-dry days, respectively. The top-left sub-panels in panels a–d indicate the vertical structure (i.e., 1000hPa-100 hPa) of the composite anomalies of the corresponding variables; and the horizontal red thick line in these sub-panels indicates the latitudinal zone of southern EMC (20°-30°N). Panels e–h are the same as the panels a–d, but for total cloud cover, 200-hPa geopotential height and wind field, 500-hPa vertical velocity, and vertical integral of moisture divergence (VIMD), respectively. The composite anomalies in panels e–h are differences in mean values for VPD-based hot-dry days relative to all summer days during 1961–2020. Panels i–l (m–p) are the same as panels e–h, but show the differences of composite anomalies computed for the years in the top tercile and the bottom tercile of VPD1 (VPD2). The claret-red dots in panels a–p indicate anomalies or differences at the 0.05 significance level based on the Student's *t*-test.

(i.e., from 1000 hPa to 200 hPa) in this region (Figure 4g and Figure S5g in Supporting Information S1), which may hinder convective activity (Cao et al., 2022). Associated with this anomalous descending motion, positive anomalies of the vertically integrated moisture divergence (VIMD) appear in southern EMC on hot-dry days (Figure 4h and Figure S5h in Supporting Information S1). The strong moisture divergence and abnormal anti-cyclone over southern EMC can block the water vapor supply from oceans such as South China Sea and Bay of Bengal, contributing to reduced atmospheric humidity and cloud cover.

We assess the difference of composite anomalies in these large-scale environmental variables computed using years in the top tercile and the bottom tercile of VPD1 (VPD2), and investigate possible reasons behind the increases in hot-dry days in southern EMC (Figures 4i and 4p). Compared to years with low VPD1/VPD2, we find less cloud cover and more solar shortwave radiation in southern EMC during years with high VPD1/VPD2 (Figures 4i and 4m). The positive geopotential height anomaly is particularly strong and extends eastward (Figure 4j), indicating an eastward extension of the South Asia High (SAH). The eastward shift of the SAH is related to the weaker Indian summer monsoon and westward shift of the Northwest Pacific subtropical high (NWPSH) (W. Wei et al., 2014). Southern EMC is thus strongly affected by the high pressure caused by the extension of the NWPSH,

which leads to the descending motion (Figures 4k and 4o) and limits water vapor advection from ocean (Figures 4l and 4p) (Luo & Lau, 2022; W. Wei et al., 2014). Furthermore, we find easterly wind anomalies prevail over the Indochina Peninsula in years with high VPD1/VPD2, opposing the climatological westerly regime of the South Asian summer monsoon (Figures 4l and 4p). This anomalous eastern wind indicates that the weak South Asian summer monsoon circulation may also be reducing moisture advection from oceans such as the South China Sea and Bay of Bengal. This wind pattern is associated with the occurrence of heatwaves in Indochina and southern EMC (Luo & Lau, 2018). The patterns of differences in large-scale circulations shown in Figures 4i-4p are consistent with those shown in Figures S5i–S5p in Supporting Information S1, using Q-based hot-dry days and Q1/Q2.

Besides the large-scale circulation anomalies on hot-dry days, we investigate the role of land-atmosphere feedbacks (Figure 5). Here, we use the evaporative fraction (EF) to link the process of atmosphere-land feedbacks. EF, defined as LE/(LE + H), where LE is surface latent heat (W/m^2) and H is surface sensible heat (W/m^2), is used as a metric to characterize the degree of land surface dryness (Costa et al., 2022; Donat et al., 2017; Ukkola et al., 2018; Ukkola et al., 2018, 2018). EF can describe the partitioning of available energy between LE and H, with low (high) values characterizing dry (wet) conditions. We find significant negative correlations ($p < 0.001$) between the region-averaged EF and all four amplification indices over southern EMC (i.e., VPD1, VPD2, Q1, and Q2; Figure 5a and Figure S6 in Supporting Information S1), suggesting that EF plays a key role in controlling changes in hot-dry days in this region. On years with larger values of the amplification indices, southern EMC is dominated by significant decreases in EF (Figure 5a and Figure S6 in Supporting Information S1), indicating that increased land surface dryness is conducive to a higher occurrence probability of hot-dry extremes in this region.

The region-averaged EF in southern EMC has a significantly positive correlation with summer-mean surface soil moisture (SSM), indicating that changes in EF are closely related to the state of summer SSM (top-left sub-panel in Figure 5b). The significantly negative anomalies of summer-mean SSM in years with low EF (Figure 5b) suggest that increased land surface dryness is strongly dominated by drying summer SSM. The summer SSM is further controlled by the initial soil moisture in the month before the summer season (i.e., May 1-m soil moisture (SM) in this study) and summer water availability (i.e., summer-mean precipitation in this study) (X. Gu et al., 2019a; X. Gu et al., 2019b). This is confirmed by the significant positive correlations between summer-mean SSM and May 1-m SM, as well as between summer-mean SSM and precipitation (see top-left sub-panels in Figures 5c and 5d). Years with low summer SSM are accompanied by lower May 1-m SM and less summer precipitation in southern EMC (Figures 5c and 5d).

Our study found precipitation is one of crucial keys to modulating hot-dry extremes from two aspects. On the one hand, summer HP can remove plenty of moisture from the air and then lead to time-mean RH decrease (Dai et al., 2020). Because of the longer time to replenish depleted moisture in the air, dry spells after HP become longer (Li, Zwiers, et al., 2021; Qiao et al., 2022) which may further drive hot extremes by land-atmosphere feedback and large-scale circulation (Miralles et al., 2019). It has been detected that the sequential HP-heatwave events have significantly increased in last 20 years across China (Y. Chen et al., 2021), which is consistent with our results. On the other hand, summer mean precipitation trends may largely affect the occurrence of compound hot and dry extremes (Bevacqua et al., 2022; Guntu et al., 2023). Summer mean precipitation, which is an important segment in land-atmosphere feedbacks, its deficits cause soil moisture depletion and in turn lead to atmospheric aridity (S. Zhou et al., 2019). The dry conditions reduce latent heat flux and help to accumulate sensible heat in the air, leading to higher air temperature (Seo et al., 2021). Therefore, decline in summer mean precipitation make it easily to create a co-occurrence of hot-dry extremes.

We use a multiple linear regression for summer-mean SSM using May 1-m SM and summer-mean precipitation, and obtain a fitted summer SSM time series (Figure 5e). The fitted summer-mean SSM is highly consistent with the original values (i.e., Spearman's $r = 0.91$, $p < 0.001$), implying that summer SSM is likely to be well predicted by May 1-m SM and summer-mean precipitation. Finally, we also use multiple linear regression for all four amplification indices using May 1-m SM and summer-mean-precipitation, in order to link these controls back to hot-dry days. The fitted amplification indices are significantly correlated with their original values (Figure 5f and Figure S7 in Supporting Information S1). The two predictors collectively can explain not only the interannual variability and but also the recent uptick in the amplification indices.

5. Additional Drivers and Areas for Further Research

In this study, we explore possible reasons for the enhanced coupling of hot and dry extremes in southern EMC. Although we focus on large-scale circulation anomalies and land-atmosphere feedbacks, the coupling of hotter

10.1029/2023EF003604

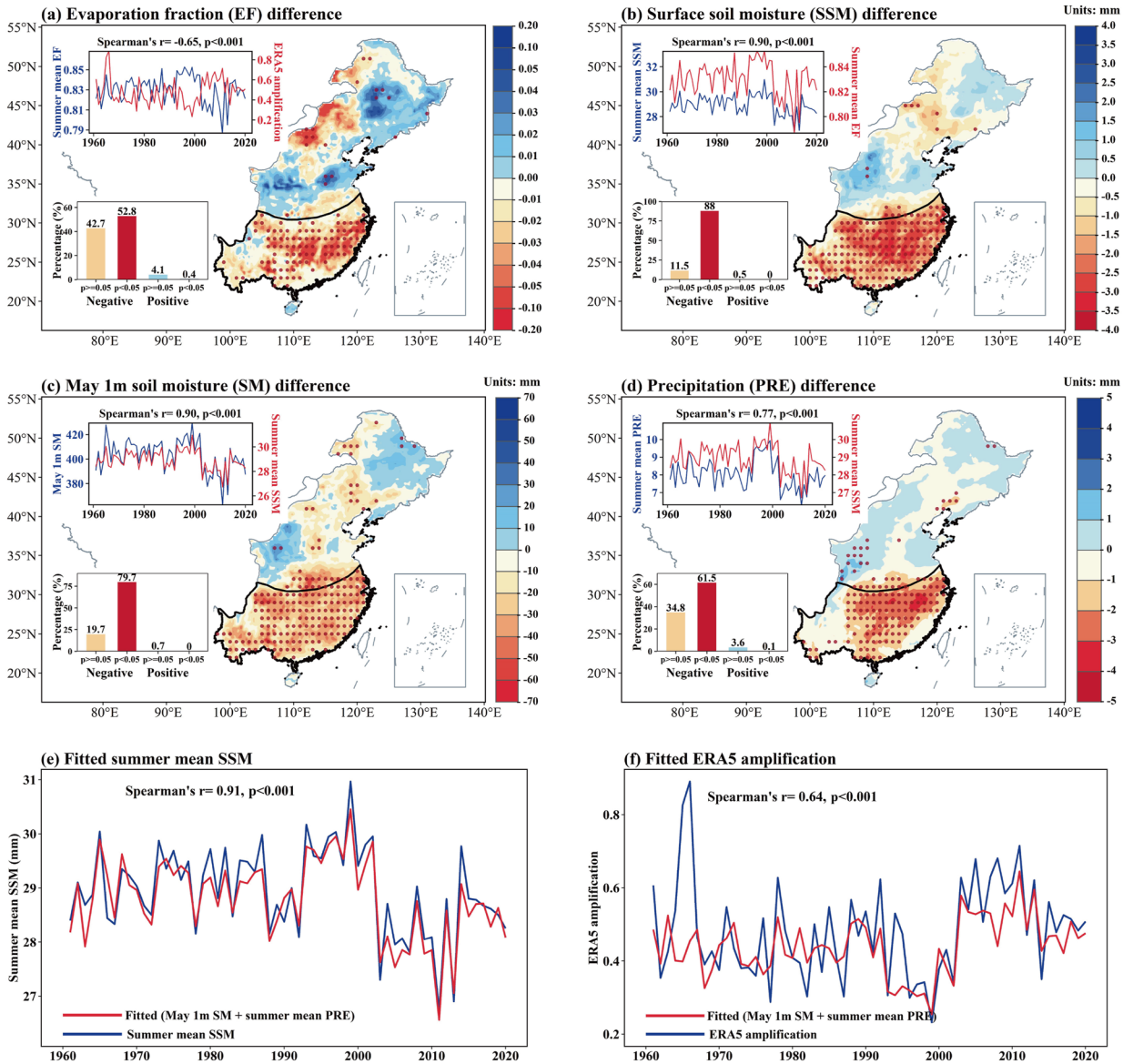

Figure 5. Land-atmosphere feedbacks linked to the stronger hot-dry coupling in southern EMC during summer seasons of 1961–2020. Panel a is the composite summer averaged evaporation fraction (EF) on years in the top tercile of VPD1 minus the bottom tercile. The blue and red time series lines in panel a indicate region-averaged EF and ERA5-based VPD1, respectively. Panel b is the composite summer surface soil moisture (SSM at top 7 cm layer) on years in the top tercile of the EF minus the bottom tercile. The blue and red lines of time series in panel b indicate region-averaged SSM and EF, respectively. Panels c and d are the composite May 1-m soil moisture (SM) and summer-mean precipitation (PRE) on years in the top tercile of the summer-mean SSM minus the bottom tercile. The blue and red time series lines in panel c (d) indicate region-averaged May 1 m SM (summer-mean precipitation) and summer-mean SSM, respectively. Panel e is the observed (blue) and fitted (red) summer-mean SSM; the fitted values are based on a multiple linear regression model using May 1 m soil moisture and summer-mean precipitation as covariates. Panel f is the same as panel e, but for ERA5-based VPD1 using May 1 m soil moisture and summer-mean precipitation.

and drier extremes may be also affected by other factors such as global warming, the contrast in land-ocean warming, and urbanization.

Under global warming, anthropogenically-driven hot extremes exhibit increasing intensity, frequency, and duration after 1960 (J. Wang et al., 2020). Increased greenhouse gas emissions lead to reduced outgoing long-wave radiation and strengthen the absorption capacity of atmosphere, further intensifying atmospheric heating (Raghuraman et al., 2021). Meanwhile, a sharp decrease in land surface relative humidity has been observed since 2000 (Simmons et al., 2010; Willett et al., 2014). Atmospheric aridity is projected to increase over the 21st century and the increase is more prominent under a higher emission scenario (Fang et al., 2022). Increasing

hot extremes and decreasing atmospheric humidity can promote the co-occurrence of hot-dry extremes. As hot extremes are projected to continue increasing, and atmospheric humidity is anticipated to decrease in the future, the frequency of hot-dry days is likely to continue increasing in a warmer climate (De Luca & Donat, 2023; Vogel et al., 2020). Future works should be conducted to quantify the role of anthropogenic warming in the enhanced coupling of hot and dry extremes in EMC region.

The contrast in land-ocean warming also affects atmospheric humidity over land (Byrne & O'Gorman, 2013b), as oceanic evaporation contributes to approximately 85% of the atmospheric water vapor over land (Trenberth et al., 2007). A theory of atmospheric dynamics suggests that near-surface moist static energy (a function of SAT and Q) uniformly changes across the tropics and fractional change in Q is roughly equal over tropical land and ocean (Byrne & O'Gorman, 2013a, 2013b; Chadwick et al., 2016; Joshi et al., 2008). Based on this theory, the warming air temperature and decreasing atmospheric humidity over tropical land are associated with weaker warming over neighboring oceans (Byrne & O'Gorman, 2018). Specifically, constrained by that land and ocean have equal fractional changes in Q, the greater warming over land than neighboring oceans leads to weakened moisture transport from oceans and then a land atmospheric drying (Byrne & O'Gorman, 2016, 2018). With the drier air over land than neighboring oceans, the land air needs to warm substantially more than the ocean air in tropical regions, in order to maintain the uniform change in the moist static energy across the tropics (Byrne, 2021). Byrne (2021) reported that the amplified warming on hot days rather than normal days over tropical land (20°S–20°N) is due to the drier air conditions on hot days. Therefore, the coupling of hotter and drier extremes in southern EMC (mostly tropical land) may be also affected by the contrast in land-ocean warming.

We also find that there are greater increases in all the four amplification indices in highly urbanized areas, such as the Yangtze River Delta (YRD) and the Pearl River Delta (PRD) (see Figures 3a–3d). In recent decades, these areas have experienced rapid urbanization and enhanced urban dry island (UDI) and urban heat island (UHI) effects due to the influence of urbanization on surface properties (Du, 2019; Kong et al., 2020; Luo & Lau, 2019; Mishra, 2015; Qian et al., 2022; Yu et al., 2022). For example, the expansion of impervious areas increases surface albedo and decreases land evaporation, which is conductive to atmospheric warming and drying synchronously in cities (J. Liu et al., 2021; Luo & Lau, 2019). The synergetic enhancement effects between UHI/UDI and heatwaves (D. Li & Bou-Zeid, 2013; Ramamurthy & Bou-Zeid, 2017; Zhao et al., 2018) can also lead to stronger coupling of hot and dry extremes in megalopolises. How urbanization affects the coupling of hot and dry extremes should be quantified in the future, but is beyond the scope of our study.

6. Conclusions

Using station-based observations and the ERA5 reanalysis data during summer seasons of 1961–2020, we investigated responses of SAT (Q/VPD) to warming temperature on dry (hot) days, detected long-term changes in the coupling of hot and dry days, and explored possible physical mechanisms behind the strong coupling of hot and dry extremes in a typical monsoon region (i.e., EMC). We find that SAT (Q/VPD) responses to warming temperature vary diversely across the Q/VPD (SAT) percentiles. Specifically, on drier (hotter) days, the warming (drying) rates become faster especially in southern EMC, which can be described simply as "drier days get hotter" ("hotter days get drier"). In other words, atmospheric warming (drying) is amplified on dry (hot) days, that is, we find strong coupling of hot and dry extremes. This coupling has become stronger in southern EMC during the past six decades, as is reflected by the increasing trends in all four amplification indices (i.e., more dry days becoming hotter and more hot days becoming drier over southern EMC).

Anomalies of large-scale circulations play an important role in the occurrence of hot-dry days and the enhanced coupling of hot and dry extremes in southern EMC. Hot-dry days are associated with less total cloud cover in southern EMC, which allows for increased solar radiation to reach the surface. Concurrently, a strong anticyclone in the upper atmosphere over China obstructs ascending air and causes a strong descending motion in southern EMC, leading to weakened convective activity. Linked to this descending motion, strong moisture divergence over southern EMC blocks the water vapor from the ocean. In southern EMC, these conditions (reduced total cloud cover, anticyclone in the upper atmosphere, abnormal descending motion, and strong moisture divergence) are significantly more prominent in years with stronger of coupling hot-dry extremes, than in years with weaker coupling of hot-dry extremes.

Another important physical mechanism which leads to stronger coupling of hotter and drier extremes in southern EMC is land-atmosphere feedbacks. Coupling of hot and dry extremes is related to changes in the partitioning

of surface heat fluxes (described by EF). Specifically, the hot-dry coupling (described by amplification indices) in southern EMC is significantly negatively related to changes in EF. In years with strong coupling of hot and dry extremes (characterized by larger amplification indices), southern EMC is dominated by reduced EF (i.e., increased land surface dryness). Changes in EF in southern EMC are significantly positively related to changes in summer-mean SSM, and years with low EF values also have dry summer SSM. The summer-mean SSM is further controlled by the initial soil moisture in the month before the summer season, as well as summer-mean precipitation. Overall, reductions in initial soil moisture and summer-mean precipitation in southern EMC lead to anomalously dry summer soil moisture linked to low evaporative fraction and result in stronger coupling of hot and dry extremes.

Data Availability Statement

The station-based observations were obtained from the National Meteorological Science Data Center available at http://data.cma.cn/en/?r=data/detail&dataCode=A.0012.0001. The ERA5 reanalysis data are available at https://www.ecmwf.int/en/forecasts/datasets/reanalysis-datasets/era5.

Acknowledgments
This work was financially supported by the National Natural Science Foundation of China (Grants 42371041, 42101052, 41901041, and 42001042), the Natural Science Foundation of Hubei Province, China (Grant 2023AFB566), the Knowledge Innovation Program of Wuhan-Shuguang (Grant 2023020201020333), the Belt and Road Special Foundation of the National Key Laboratory of Water Disaster Prevention (Grant 2022nkms03), the CRSRI Open Research Program (Grant CKWV20231194/KY), the open funding from Key Laboratory of Meteorological Disaster Ministry of Education & Collaborative Innovation Center on Forecast and Evaluation of Meteorological Disasters, Nanjing University of Information Science & Technology (Grant KLME202308), the Pre-research Project of SongShan Laboratory (Grant YYYY062022001), and the open funding from the Institute of Arid Meteorology, China Meteorological Administration, Lanzhou (Grant IAM202214).

References

Bell, B., Hersbach, H., Simmons, A., Berrisford, P., Dahlgren, P., Horányi, A., et al. (2021). The ERA5 global reanalysis: Preliminary extension to 1950. *Quarterly Journal of the Royal Meteorological Society*, *147*(741), 4186–4227. https://doi.org/10.1002/qj.4174

Berg, A., Findell, K., Lintner, B., Giannini, A., Seneviratne, S. I., Van den Hurk, B., et al. (2016). Land–atmosphere feedbacks amplify aridity increase over land under global warming. *Nature Climate Change*, *6*(9), 869–874. https://doi.org/10.1038/nclimate3029

Bevacqua, E., Zappa, G., Lehner, F., & Zscheischler, J. (2022). Precipitation trends determine future occurrences of compound hot–dry events. *Nature Climate Change*, *12*(4), 350–355. https://doi.org/10.1038/s41558-022-01309-5

Bolton, D. (1980). The computation of equivalent potential temperature. *Monthly Weather Review*, *108*(7), 1046–1053. https://doi.org/10.1175/1520-0493(1980)108<1046:tcoept>2.0.co;2

Bourdin, S., Kluft, L., & Stevens, B. (2021). Dependence of climate sensitivity on the given distribution of relative humidity. *Geophysical Research Letters*, *48*(8). https://doi.org/10.1029/2021GL092462

Byrne, M. P. (2021). Amplified warming of extreme temperatures over tropical land. *Nature Geoscience*, *14*(11), 837–841. https://doi.org/10.1038/s41561-021-00828-8

Byrne, M. P., & O'Gorman, P. A. (2013a). Land–Ocean warming contrast over a wide range of climates: Convective quasi-equilibrium theory and idealized simulations. *Journal of Climate*, *26*(12), 4000–4016. https://doi.org/10.1175/JCLI-D-12-00262.1

Byrne, M. P., & O'Gorman, P. A. (2013b). Link between land-ocean warming contrast and surface relative humidities in simulations with coupled climate models. *Geophysical Research Letters*, *40*(19), 5223–5227. https://doi.org/10.1002/grl.50971

Byrne, M. P., & O'Gorman, P. A. (2016). Understanding decreases in land relative humidity with global warming: Conceptual model and GCM simulations. *Journal of Climate*, *29*(24), 9045–9061. https://doi.org/10.1175/JCLI-D-16-0351.1

Byrne, M. P., & O'Gorman, P. A. (2018). Trends in continental temperature and humidity directly linked to ocean warming. *Proceedings of the National Academy of Sciences*, *115*(19), 4863–4868. https://doi.org/10.1073/pnas.1722312115

Cai, J., Zhang, Y., Li, Y., Liang, X., & Jiang, T. (2017). Analyzing the characteristics of soil moisture using GLDAS data: A case study in eastern China. *Applied Sciences*, *7*(6), 566. https://doi.org/10.3390/app7060566

Cao, B., Lyu, S., Zhang, Y., Yang, X., Li, B., Yuan, L., & Li, M. (2022). Factors influencing diurnal variations of cloud and precipitation in the Yushu area of the Tibetan plateau. *Journal of Meteorological Research*, *36*(2), 311–325. https://doi.org/10.1007/s13351-022-1167-6

Cao, L., Zhu, Y., Tang, G., Yuan, F., & Yan, Z. (2016). Climatic warming in China according to a homogenized data set from 2419 stations: Climatic warming in China. *International Journal of Climatology*, *36*(13), 4384–4392. https://doi.org/10.1002/joc.4639

Chadwick, R., Good, P., & Willett, K. (2016). A simple moisture advection model of specific humidity change over land in response to SST warming. *Journal of Climate*, *29*(21), 7613–7632. https://doi.org/10.1175/JCLI-D-16-0241.1

Chen, R., Wen, Z., & Lu, R. (2018). Large-scale circulation anomalies and intraseasonal oscillations associated with long-lived extreme heat events in South China. *Journal of Climate*, *31*(1), 213–232. https://doi.org/10.1175/JCLI-D-17-0232.1

Chen, X., Su, Y., Liao, J., Shang, J., Dong, T., Wang, C., et al. (2016). Detecting significant decreasing trends of land surface soil moisture in eastern China during the past three decades (1979–2010). *Journal of Geophysical Research: Atmospheres*, *121*(10), 5177–5192. https://doi.org/10.1002/2015JD024676

Chen, Y., Liao, Z., Shi, Y., Tian, Y., & Zhai, P. (2021). Detectable increases in sequential flood-heatwave events across China during 1961–2018. *Geophysical Research Letters*, *10*(6). https://doi.org/10.1029/2021gl092549

Chen, Y., & Zhai, P. (2017). Revisiting summertime hot extremes in China during 1961-2015: Overlooked compound extremes and significant changes: Overlooked Changes of Hot Extremes. *Geophysical Research Letters*, *44*(10), 5096–5103. https://doi.org/10.1002/2016GL072281

Chen, Y., Zhai, P., & Zhou, B. (2018). Detectable impacts of the past half-degree global warming on summertime hot extremes in China. *Geophysical Research Letters*, *45*(14), 7130–7139. https://doi.org/10.1029/2018GL079216

Costa, D. F., Gomes, H. B., Silva, M. C. L., & Zhou, L. (2022). The most extreme heat waves in Amazonia happened under extreme dryness. *Climate Dynamics*, *59*(1–2), 281–295. https://doi.org/10.1007/s00382-021-06134-8

Dai, A., Rasmussen, R. M., Liu, C., Ikeda, K., & Prein, A. F. (2020). A new mechanism for warm-season precipitation response to globalwarming based on convection-permitting simulations. *Climate Dynamics*, *55*(1–2), 343–368. https://doi.org/10.1007/s00382-017-3787-6

Dannenberg, M. P., Yan, D., Barnes, M. L., Smith, W. K., Johnston, M. R., Scott, R. L., et al. (2022). Exceptional heat and atmospheric dryness amplified losses of primary production during the 2020 U.S. Southwest hot drought. *Global Change Biology*, *28*(16), 4794–4806. https://doi.org/10.1111/gcb.16214

De Luca, P., & Donat, M. G. (2023). Projected changes in hot, dry, and compound hot-dry extremes over global land regions. *Geophysical Research Letters*, *50*(13), e2022GL102493. https://doi.org/10.1029/2022GL102493

Donat, M. G., Pitman, A. J., & Seneviratne, S. I. (2017). Regional warming of hot extremes accelerated by surface energy fluxes. *Geophysical Research Letters*, *44*(13), 7011–7019. https://doi.org/10.1002/2017GL073733
Du, J., Wang, K., Jiang, S., Cui, B., Wang, J., & Zhao, C. (2019). Urban dry island effect mitigated urbanization effect on observed warming in China. *Journal of Climate*, *32*(18), 19–5723. https://doi.org/10.1175/jcli-d-18-0712.1
Espinoza, J. C., Ronchail, J., Marengo, J. A., & Segura, H. (2019). Contrasting North–South changes in Amazon wet-day and dry-day frequency and related atmospheric features (1981–2017). *Climate Dynamics*, *52*(9–10), 5413–5430. https://doi.org/10.1007/s00382-018-4462-2
Fang, Z., Zhang, W., Brandt, M., Abdi, A. M., & Fensholt, R. (2022). Globally increasing atmospheric aridity over the 21st century. *Earth's Future*, *10*(10). https://doi.org/10.1029/2022EF003019
Feng, S., Gu, X., Luo, S., Liu, R., Gulakhmadov, A., Slater, L. J., et al. (2022). Greenhouse gas emissions drive global dryland expansion but not spatial patterns of change in aridification. *Journal of Climate*, *35*(20), 2901–2917. https://doi.org/10.1175/JCLI-D-22-0103.1
Gu, L., Chen, J., Yin, J., Slater, L. J., Wang, H., Guo, Q., et al. (2022). Global increases in compound flood-hot extreme Hazards under climate warming. *Geophysical Research Letters*, *49*(8). https://doi.org/10.1029/2022GL097726
Gu, X., Zhang, Q., Li, J., Chen, D., Singh, V. P., Zhang, Y., et al. (2020). Impacts of anthropogenic warming and uneven regional socio-economic development on global river flood risk. *Journal of Hydrology*, *590*, 125262. https://doi.org/10.1016/j.jhydrol.2020.125262
Gu, X., Zhang, Q., Li, J., Singh, V. P., Liu, J., Sun, P., & Cheng, C. (2019a). Attribution of global soil moisture drying to human activities: A quantitative viewpoint. *Geophysical Research Letters*, *46*(5), 2573–2582. https://doi.org/10.1029/2018GL080768
Gu, X., Zhang, Q., Li, J., Singh, V. P., Liu, J., Sun, P., et al. (2019b). Intensification and expansion of soil moisture drying in warm season over Eurasia under global warming. *Journal of Geophysical Research: Atmospheres*, *124*(7), 3765–3782. https://doi.org/10.1029/2018JD029776
Gu, X., Zhang, Q., Singh, V. P., & Shi, P. (2017). Changes in magnitude and frequency of heavy precipitation across China and its potential links to summer temperature. *Journal of Hydrology*, *547*, 718–731. https://doi.org/10.1016/j.jhydrol.2017.02.041
Guntu, R. K., Merz, B., & Agarwal, A. (2023). Increased likelihood of compound dry and hot extremes in India. *Atmospheric Research*, *290*, 106789. https://doi.org/10.1016/j.atmosres.2023.106789
Hamed, K. H., & Ramachandra Rao, A. (1998). A modified Mann-Kendall trend test for autocorrelated data. *Journal of Hydrology*, *204*(1–4), 182–196. https://doi.org/10.1016/S0022-1694(97)00125-X
Held, I. M., & Soden, B. J. (2006). Robust responses of the hydrological cycle to global warming. *Journal of Climate*, *19*(21), 16–5699. https://doi.org/10.1175/jcli3990.1
Hersbach, H., Bell, B., Berrisford, P., Hirahara, S., Horányi, A., Muñoz-Sabater, J., et al. (2020). The ERA5 global reanalysis. *Quarterly Journal of the Royal Meteorological Society*, *146*(730), 1999–2049. https://doi.org/10.1002/qj.3803
Horton, R. M., Mankin, J. S., Lesk, C., Coffel, E., & Raymond, C. (2016). A review of recent advances in research on extreme heat events. *Current Climate Change Reports*, *2*(4), 242–259. https://doi.org/10.1007/s40641-016-0042-x
Huang, X., Hao, L., Sun, G., Yang, Z., Li, W., & Chen, D. (2022). Urbanization aggravates effects of global warming on local atmospheric drying. *Geophysical Research Letters*, *49*(2). https://doi.org/10.1029/2021GL095709
Ji, H., Feng, A., Zhao, Y., Liao, J., Zhang, Z., Gu, C., & Feng, A. (2023). Characteristics of heat waves in mainland China since 1961 based on absolute and relative methods. *Atmosphere*, *14*(3), 544. https://doi.org/10.3390/atmos14030544
Joshi, M. M., Gregory, J. M., Webb, M. J., Sexton, D. M. H., & Johns, T. C. (2008). Mechanisms for the land/sea warming contrast exhibited by simulations of climate change. *Climate Dynamics*, *30*(5), 455–465. https://doi.org/10.1007/s00382-007-0306-1
Kong, D., Gu, X., Li, J., Ren, G., & Liu, J. (2020). Contributions of global warming and urbanization to the Intensification of human-perceived heatwaves over China. *Journal of Geophysical Research: Atmospheres*, *125*(18). https://doi.org/10.1029/2019JD032175
Li, C., Gu, X., Bai, W., Slater, L. J., Li, J., Kong, D., et al. (2021). Asymmetric response of short- and long-duration dry spells to warming during the warm-rain season over Eastern monsoon China. *Journal of Hydrology*, *603*, 127114. https://doi.org/10.1016/j.jhydrol.2021.127114
Li, C., Gu, X., Slater, L. J., Liu, J., Li, J., Zhang, X., & Kong, D. (2022). Urbanization-induced increases in heavy precipitation are magnified by moist heatwaves in an urban agglomeration of East China. *Journal of Climate*, *36*(2), 1–37. https://doi.org/10.1175/JCLI-D-22-0223.1
Li, C., Zwiers, F., Zhang, X., Li, G., Sun, Y., & Wehner, M. (2021). Changes in annual extremes of daily temperature and precipitation in CMIP6 models. *Journal of Climate*, *34*(9), 3441–3460. https://doi.org/10.1175/JCLI-D-19-1013.1
Li, D., & Bou-Zeid, E. (2013). Synergistic interactions between urban heat islands and heat waves: The impact in cities is larger than the sum of its parts. *Journal of Applied Meteorology and Climatology*, *52*(9), 2051–2064. https://doi.org/10.1175/JAMC-D-13-02.1
Liang, L., Yu, L., & Wang, Z. (2022). Identifying the dominant impact factors and their contributions to heatwave events over mainland China. *Science of the Total Environment*, *848*, 157527. https://doi.org/10.1016/j.scitotenv.2022.157527
Liao, Z., Chen, Y., Li, W., & Zhai, P. (2021). Growing threats from unprecedented sequential flood-hot extremes across China. *Geophysical Research Letters*, *48*(18). https://doi.org/10.1029/2021GL094505
Liu, J., You, Y., Li, J., Sitch, S., Gu, X., Nabel, J. E. M. S., et al. (2021). Response of global land evapotranspiration to climate change, elevated CO2, and land use change. *Agricultural and Forest Meteorology*, *311*, 108663. https://doi.org/10.1016/j.agrformet.2021.108663
Liu, L., Gudmundsson, L., Hauser, M., Qin, D., Li, S., & Seneviratne, S. I. (2020). Soil moisture dominates dryness stress on ecosystem production globally. *Nature Communications*, *11*(1), 4892. https://doi.org/10.1038/s41467-020-18631-1
Liu, X., Tang, Q., Zhang, X., Groisman, P., Sun, S., Lu, H., & Li, Z. (2017). Spatially distinct effects of preceding precipitation on heat stress over eastern China. *Environmental Research Letters*, *12*(11), 115010. https://doi.org/10.1088/1748-9326/aa88f8
Luo, M., & Lau, N. (2019). Urban expansion and drying climate in an urban agglomeration of East China. *Geophysical Research Letters*, *46*(12), 6868–6877. https://doi.org/10.1029/2019GL082736
Luo, M., & Lau, N.-C. (2017). Heat waves in southern China: Synoptic behavior, long-term change, and urbanization effects. *Journal of Climate*, *30*(2), 703–720. https://doi.org/10.1175/JCLI-D-16-0269.1
Luo, M., & Lau, N.-C. (2018). Synoptic characteristics, atmospheric controls, and long-term changes of heat waves over the Indochina Peninsula. *Climate Dynamics*, *51*(7–8), 2707–2723. https://doi.org/10.1007/s00382-017-4038-6
Luo, M., Lau, N.-C., & Liu, Z. (2022). Different mechanisms for daytime, nighttime, and compound heatwaves in southern China. *Weather and Climate Extremes*, *36*, 100449. https://doi.org/10.1016/j.wace.2022.100449
Luo, M., Wu, S., Liu, Z., & Lau, N. (2022). Contrasting circulation patterns of dry and humid heatwaves over southern China. *Geophysical Research Letters*, *49*(16). https://doi.org/10.1029/2022GL099243
Massey, F. J. (1951). The Kolmogorov-Smirnov test for goodness of fit. *Journal of the American Statistical Association*, *46*(253), 68–78. https://doi.org/10.1080/01621459.1951.10500769
Mazdiyasni, O., & AghaKouchak, A. (2015). Substantial increase in concurrent droughts and heatwaves in the United States. *Earth, Atmospheric, and Planetary Sciences*, *112*(37), 11484–11489.
McElhinny, M., Beckers, J. F., Hanes, C., Flannigan, M., & Jain, P. (2020). A high-resolution reanalysis of global fire weather from 1979 to 2018 – Overwintering the drought code. *Earth System Science Data*, *12*(3), 1823–1833. https://doi.org/10.5194/essd-12-1823-2020

McKinnon, K. A., & Poppick, A. (2020). Estimating changes in the observed relationship between humidity and temperature using noncrossing quantile smoothing splines. *Journal of Agricultural, Biological, and Environmental Statistics*, *25*(3), 292–314. https://doi.org/10.1007/s13253-020-00393-4

McKinnon, K. A., Poppick, A., & Simpson, I. R. (2021). Hot extremes have become drier in the United States Southwest. *Nature Climate Change*, *11*(7), 598–604. https://doi.org/10.1038/s41558-021-01076-9

Miralles, D. G., Gentine, P., Seneviratne, S. I., & Teuling, A. J. (2019). Land-atmospheric feedbacks during droughts and heatwaves: State of the science and current challenges: Land feedbacks during droughts and heatwaves. *Annals of the New York Academy of Sciences*, *1436*(1), 19–35. https://doi.org/10.1111/nyas.13912

Miralles, D. G., Teuling, A. J., Van Heerwaarden, C. C., & Vilà-Guerau de Arellano, J. (2014). Mega-heatwave temperatures due to combined soil desiccation and atmospheric heat accumulation. *Nature Geoscience*, *7*(5), 345–349. https://doi.org/10.1038/ngeo2141

Mishra, V., Ambika, A. K., Asoka, A., Aadhar, S., Buzan, J., Kumar, R., & Huber, M. (2020). Moist heat stress extremes in India enhanced by irrigation. *Nature Geoscience*, *13*(11), 722–728. https://doi.org/10.1038/s41561-020-00650-8

Mishra, V., Ganguly, A. R., Nijssen, B., & Lettenmaier, D. P. (2015). Changes in observed climate extremes in global urban areas. *Environmental Research Letters*, *11*(2), 024005. https://doi.org/10.1088/1748-9326/10/2/024005

Mukherjee, S., & Mishra, A. K. (2021). Increase in compound drought and heatwaves in a warming world. *Geophysical Research Letters*, *48*(1), e2020GL090617. https://doi.org/10.1029/2020GL090617

Murari, K. K., Ghosh, S., Patwardhan, A., Daly, E., & Salvi, K. (2015). Intensification of future severe heat waves in India and their effect on heat stress and mortality. *Regional Environmental Change*, *15*(4), 569–579. https://doi.org/10.1007/s10113-014-0660-6

Ning, G., Luo, M., Wang, S., Liu, Z., Wang, P., & Yang, Y. (2022). Dominant modes of summer wet bulb temperature in China. *Climate Dynamics*, *59*(5–6), 1473–1488. https://doi.org/10.1007/s00382-021-06051-w

Park, C.-E., Jeong, S.-J., Ho, C.-H., Park, H., Piao, S., Kim, J., & Feng, S. (2017). Dominance of climate warming effects on recent drying trends over wet monsoon regions. *Atmospheric Chemistry and Physics*, *17*(17), 10467–10476. https://doi.org/10.5194/acp-17-10467-2017

Perkins, S. E. (2015). A review on the scientific understanding of heatwaves—Their measurement, driving mechanisms, and changes at the global scale. *Atmospheric Research*, *164–165*, 242–267. https://doi.org/10.1016/j.atmosres.2015.05.014

Pfahl, S., Schwierz, C., Croci-Maspoli, M., Grams, C. M., & Wernli, H. (2015). Importance of latent heat release in ascending air streams for atmospheric blocking. *Nature Geoscience*, *8*(8), 610–614. https://doi.org/10.1038/ngeo2487

Pfahl, S., & Wernli, H. (2012). Quantifying the relevance of atmospheric blocking for co-located temperature extremes in the Northern Hemisphere on (sub-)daily time scales: Blocking and temperature extremes. *Geophysical Research Letters*, *39*(12). https://doi.org/10.1029/2012gl052261

Qian, Y., Chakraborty, T., Li, J., Li, D., He, C., Sarangi, C., et al. (2022). Urbanization impact on regional climate and extreme weather: Current understanding, uncertainties. *Future Research Directions*, *39*, 42. https://doi.org/10.1007/s00376-021-1371-9

Qiao, Y., Xu, W., Wu, D., Meng, C., Qin, L., Li, Z., & Zhang, X. (2022). Changes in the spatiotemporal patterns of dry/wet abrupt alternation frequency, duration, and severity in Mainland China, 1980–2019. *Science of the Total Environment*, *838*, 156521. https://doi.org/10.1016/j.scitotenv.2022.156521

Qing, Y., Wang, S., Ancell, B. C., & Yang, Z.-L. (2022). Accelerating flash droughts induced by the joint influence of soil moisture depletion and atmospheric aridity. *Nature Communications*, *13*(1), 1139. https://doi.org/10.1038/s41467-022-28752-4

Raghuraman, S. P., Paynter, D., & Ramaswamy, V. (2021). Anthropogenic forcing and response yield observed positive trend in Earth's energy imbalance. *Nature Communications*, *12*(1), 4577. https://doi.org/10.1038/s41467-021-24544-4

Ramamurthy, P., & Bou-Zeid, E. (2017). Heatwaves and urban heat islands: A comparative analysis of multiple cities: Heatwaves and urban heat islands. *Journal of Geophysical Research: Atmospheres*, *122*(1), 168–178. https://doi.org/10.1002/2016JD025357

Ren, G., Li, J., Ren, Y., Chu, Z., Zhang, A., Zhou, Y., et al. (2015). An integrated procedure to determine a reference station network for evaluating and adjusting urban bias in surface air temperature data. *Journal of Applied Meteorology and Climatology*, *54*(6), 1248–1266. https://doi.org/10.1175/JAMC-D-14-0295.1

Seneviratne, S. I., Corti, T., Davin, E. L., Hirschi, M., Jaeger, E. B., Lehner, I., et al. (2010). Investigating soil moisture–climate interactions in a changing climate: A review. *Earth-Science Reviews*, *99*(3–4), 125–161. https://doi.org/10.1016/j.earscirev.2010.02.004

Seo, Y.-W., Ha, K.-J., & Park, T.-W. (2021). Feedback attribution to dry heatwaves over East Asia. *Environmental Research Letters*, *16*(6), 064003. https://doi.org/10.1088/1748-9326/abf18f

Simmons, A. J., Willett, K. M., Jones, P. D., Thorne, P. W., & Dee, D. P. (2010). Low-frequency variations in surface atmospheric humidity, temperature, and precipitation: Inferences from reanalyses and monthly gridded observational data sets. *Journal of Geophysical Research*, *115*(D1), D01110. https://doi.org/10.1029/2009JD012442

Singh, D., Tsiang, M., Rajaratnam, B., & Diffenbaugh, N. S. (2014). Observed changes in extreme wet and dry spells during the South Asian summer monsoon season. *Nature Climate Change*, *4*(6), 456–461. https://doi.org/10.1038/nclimate2208

Sippel, S., Meinshausen, N., Fischer, E. M., Székely, E., & Knutti, R. (2020). Climate change now detectable from any single day of weather at global scale. *Nature Climate Change*, *10*(1), 35–41. https://doi.org/10.1038/s41558-019-0666-7

Sun, D.-Z., & Oort, A. H. (1995). Humidity–temperature relationships in the tropical troposphere. *Journal of Climate*, *8*(8), 1974–1987. https://doi.org/10.1175/1520-0442(1995)008<1974:hrittt>2.0.co;2

Sun, Y., Zhang, X., Zwiers, F. W., Song, L., Wan, H., Hu, T., et al. (2014). Rapid increase in the risk of extreme summer heat in Eastern China. *Nature Climate Change*, *4*(12), 1082–1085. https://doi.org/10.1038/nclimate2410

Tabari, H., & Willems, P. (2023). Global risk assessment of compound hot-dry events in the context of future climate change and socioeconomic factors. *NPJ Climate and Atmospheric Science*, *6*(1), 74. https://doi.org/10.1038/s41612-023-00401-7

Trenberth, K. E., Smith, L., Qian, T., Dai, A., & Fasullo, J. (2007). Estimates of the global water budget and its annual cycle using observational and model data. *Journal of Hydrometeorology*, *8*(4), 758–769. https://doi.org/10.1175/JHM600.1

Tripathy, K. P., Mukherjee, S., Mishra, A. K., Mann, M. E., & Williams, A. P. (2023). Climate change will accelerate the high-end risk of compound drought and heatwave events. *Proceedings of the National Academy of Sciences*, *120*(28), e2219825120. https://doi.org/10.1073/pnas.2219825120

Ukkola, A. M., Pitman, A. J., Donat, M. G., De Kauwe, M. G., & Angélil, O. (2018). Evaluating the contribution of land-atmosphere coupling to heat extremes in CMIP5 models. *Geophysical Research Letters*, *45*(17), 9003–9012. https://doi.org/10.1029/2018GL079102

Vogel, M. M., Hauser, M., & Seneviratne, S. I. (2020). Projected changes in hot, dry and wet extreme events' clusters in CMIP6 multi-model ensemble. *Environmental Research Letters*, *15*(9), 094021. https://doi.org/10.1088/1748-9326/ab90a7

Wang, B., Liu, J., Kim, H.-J., Webster, P. J., & Yim, S.-Y. (2012). Recent change of the global monsoon precipitation (1979–2008). *Climate Dynamics*, *39*(5), 1123–1135. https://doi.org/10.1007/s00382-011-1266-z

Wang, J., Chen, Y., Tett, S. F. B., Yan, Z., Zhai, P., Feng, J., & Xia, J. (2020). Anthropogenically-driven increases in the risks of summertime compound hot extremes. *Nature Communications*, *11*(1), 528. https://doi.org/10.1038/s41467-019-14233-8

Wang, L., Wang, W. J., Du, H., Shen, X., Wu, Z., Ma, S., et al. (2022). Was warming amplified under drought conditions across China in observations and future projections? *Earth's Future*, *10*(3). https://doi.org/10.1029/2021EF002614

Wang, P., Tong, X., Qiu, J., Chen, Y., Wu, S., Chan, T. O., et al. (2022). Amplification effect of urbanization on atmospheric aridity over China under past global warming. *Earth's Future*, *10*(5). https://doi.org/10.1029/2021EF002335

Wang, X., He, L., Ma, X., Bie, Q., Luo, L., Xiong, Y., & Ye, J. (2022). The emergence of prolonged deadly humid heatwaves. *International Journal of Climatology*, *42*(16), 7750–8618. https://doi.org/10.1002/joc.7750

Wei, L., Gu, X., Kong, D., & Liu, J. (2021). A long-term perspective of hydroclimatological impacts of tropical cyclones on regional heavy precipitation over eastern monsoon China. *Atmospheric Research*, *264*, 105862. https://doi.org/10.1016/j.atmosres.2021.105862

Wei, W., Zhang, R., Wen, M., Rong, X., & Li, T. (2014). Impact of Indian summer monsoon on the South Asian High and its influence on summer rainfall over China. *Climate Dynamics*, *43*(5–6), 1257–1269. https://doi.org/10.1007/s00382-013-1938-y

Willett, K. M., Dunn, R. J. H., Thorne, P. W., Bell, S., De Podesta, M., Parker, D. E., et al. (2014). HadISDH land surface multi-variable humidity and temperature record for climate monitoring. *Climate of the Past*, *10*(6), 1983–2006. https://doi.org/10.5194/cp-10-1983-2014

Wu, Y., Ji, H., Wen, J., Wu, S.-Y., Xu, M., Tagle, F., et al. (2019). The characteristics of regional heavy precipitation events over eastern monsoon China during 1960–2013. *Global and Planetary Change*, *172*, 414–427. https://doi.org/10.1016/j.gloplacha.2018.11.001

Xie, W., Zhou, B., You, Q., Zhang, Y., & Ullah, S. (2020). Observed changes in heat waves with different severities in China during 1961–2015. *Theoretical and Applied Climatology*, *141*(3–4), 1529–1540. https://doi.org/10.1007/s00704-020-03285-2

Xie, Y., Liu, Y., & Huang, J. (2016). Overestimated Arctic warming and underestimated Eurasia mid-latitude warming in CMIP5 simulations: Overestimated Arctic and underestimated mid-latitude warming in CMIP5. *International Journal of Climatology*, *36*(14), 4475–4487. https://doi.org/10.1002/joc.4644

Xu, F., Chan, T. O., & Luo, M. (2021). Different changes in dry and humid heat waves over China. *International Journal of Climatology*, *41*(2), 1369–1382. https://doi.org/10.1002/joc.6815

Yao, Y., Zhang, W., & Kirtman, B. (2023). Increasing impacts of summer extreme precipitation and heatwaves in eastern China. *Climatic Change*, *176*(10), 131. https://doi.org/10.1007/s10584-023-03610-4

You, Q., Jiang, Z., Kong, L., Wu, Z., Bao, Y., Kang, S., & Pepin, N. (2017). A comparison of heat wave climatologies and trends in China based on multiple definitions. *Climate Dynamics*, *48*(11–12), 3975–3989. https://doi.org/10.1007/s00382-016-3315-0

Yu, X., Gu, X., Kong, D., Zhang, Q., Cao, Q., Slater, L. J., et al. (2022). Asymmetrical shift toward less light and more heavy precipitation in an urban agglomeration of East China: Intensification by urbanization. *Geophysical Research Letters*, *49*(4). https://doi.org/10.1029/2021GL097046

Zhang, W., Zhou, T., Zou, L., Zhang, L., & Chen, X. (2018). Reduced exposure to extreme precipitation from 0.5°C less warming in global land monsoon regions. *Nature Communications*, *9*(1), 3153. https://doi.org/10.1038/s41467-018-05633-3

Zhao, L., Oppenheimer, M., Zhu, Q., Baldwin, J. W., Ebi, K. L., Bou-Zeid, E., et al. (2018). Interactions between urban heat islands and heat waves. *Environmental Research Letters*, *13*(3), 034003. https://doi.org/10.1088/1748-9326/aa9f73

Zhou, B., Xu, Y., Wu, J., Dong, S., & Shi, Y. (2016). Changes in temperature and precipitation extreme indices over China: Analysis of a high-resolution grid dataset. *International Journal of Climatology*, *36*(3), 1051–1066. https://doi.org/10.1002/joc.4400

Zhou, S., Williams, A. P., Berg, A. M., Cook, B. I., Zhang, Y., Hagemann, S., et al. (2019b). Land–atmosphere feedbacks exacerbate concurrent soil drought and atmospheric aridity. *Proceedings of the National Academy of Sciences*, *116*(38), 18848–18853. https://doi.org/10.1073/pnas.1904955116

Zhou, S., Williams, A. P., Berg, A. M., Cook, B. I., Zhang, Y., Hagemann, S., et al. (2019a). Land–atmosphere feedbacks exacerbate concurrent soil drought and atmospheric aridity. *Earth, Atmospheric, and Planetary Sciences*, *116*(38), 18848–18853.

Zhou, S., Zhang, Y., Park Williams, A., & Gentine, P. (2019). Projected increases in intensity, frequency, and terrestrial carbon costs of compound drought and aridity events. *Science Advances*, *5*(1), eaau5740. https://doi.org/10.1126/sciadv.aau5740